2013 IEEE 11th Malaysia International Conference on Communications
26th - 28th November 2013, Kuala Lumpur, Malaysia

Improving The Capacity of Channels For Multi-Path, Indoor, Ultra-Wideband Wireless Systems

Rashid A. Fayadh[1], F. Malek[2], Hilal A. Fadhil[3], Norshafinash Suadin[4]

University Malaysia Perlis (UniMAP)[1]
School of Computer and Communication Engineering
Arau, Perlis Malaysia
r_rashid47@yahoo.com

University Malaysia Perlis (UniMAP)[3]
School of Computer and Communication Engineering
Arau, Perlis, Malaysia
hilaladnan@unimap.edu.my

University Malaysia Perlis (UniMAP)[2]
School of Electrical System Engineering
Arau, Perlis, Malaysia
mfareq@unimap.edu.my

University Malaysia Perlis (UniMAP)[4]
School of Electrical System Engineering
Arau, Perlis, Malaysia
norshafinash@unimap.edu.my

A

Abstract—**The scattering and reflections that occur-during indoor propagation create serious problems for multi-path channel transmissions due to seriously suffering from plenty of resolvable multipath components (MPCs) through line of sight (LOS) and non-line of sight (NLOS) environments. This high-gain antenna can be used to evaluate indoor, single-in single-out (SISO) and multiple-in multiple-out (MIMO) UWB systems. The high-gain antenna gives a more powerful link that can transmit and receive more data at a faster rate while mitigating interference. The capacities of the channels for these wireless systems and the advantages of using multiple antennas rather than a single antenna are presented.**

***Keywords— ultra wideband technologies; single-input single-output (SISO); multiple-input multiple-output (MIMO); indoor multipath propagation*.**

I. INTRODUCTION

At the present time, UWB technologies have great potential for use in home networks wireless personal area networks (WPANs) because they can overcome the obstacles that cause high attenuation, such as concrete walls, furniture, and human bodies. In [1], a packet-level UWB channel model was built as a human-blocking model to facilitate the analysis of the quality of service (QoS) of a UWB network. Another study has been published by [2] using partitions made of different materials that had different values of SNR on MIMO and SISO-UWB transmission to improve the capacity of the channel. A spatial multiplexing was used to employ the MIMO systems depending on multipath wireless channel [3], [4]. In [5], the ultra-wideband channel capacity was improved depending on measured data. In this paper, we focus on channel capacity of multipath systems with single or multiple transmit and receive antennas, so that a small and high gain antenna (20 x 25 x 1) mm^3 was based in this work which was proposed in [6] to give reliability for using an array of UWB antennas in indoor propagation systems. Also there are three prototype models were shown in [7] for the planar triangular, monopole antennas can be used in this research to convert a single-band antenna to a dual-band antenna used by WLAN, so these techniques support the use of single antenna systems because more resonance frequencies can be obtained.

In this paper, we concentrated on the increasing the channel capacity bit rate using high gain ultra wideband antenna that provided the channel capacity required for indoor wireless systems that have single or multiple transmitting or receiving antennas. The application of this antenna was tested on a wireless, multi-path channel to insure that it provided the theoretically-calculated channel capacity, which is directly proportional to the cumulative distribution probability. The contributions of this work lies on section II of the transmitting signal configuration and section III of the received power for high gain antenna. Section IV, section V, and section VI are dealing with FCC indoor channel models, channel capacity for single/multiple antennas, and the discussion of simulated results, respectively, while section VII concentrates on conclusion.

II. UWB TRANSMITTED SIGNAL

The UWB technology refers to a short impulse with a very fast communication scheme. According to the FCC's report, the fractional bandwidth can be calculated as follows:

$$\text{Fractional Bandwidth} = 2(f_H - f_L)/(f_H + f_L) \quad (1)$$

where, f_H and f_L are the upper and lower frequencies, respectively, and the dynamic range of -10dB from -41.3dBm/MHz power emission level that give 7.5 GHz (3.1-10.6GHz) bandwidth. Compared with a narrow-band system, the effects of a multi-path system are mitigated because of the short pulses that provide a high data-rate performance in multi-user detection. A UWB system can support many channels with fractional technology as in a personal area network (PAN), local area network (LAN), and wide area network (WAN) [8].

The main spread-spectrum techniques in UWB communication are called direct-sequence UWB (DS-UWB) and time-hopping UWB (TH-UWB). In a DS-UWB system, pseudo-random (PR) code is used to spread the information symbols by transmitting continuous pulses. In this research, binary phase shift keying (BPSK) modulation was used to modulate the transmitted binary symbol (d_j) over the j^{th} form

978-1-4799-1532-3/13/$31.00 ©2013 IEEE

interval that spread by the multiple mono-cycle sequence, so the transmitted signal format is illustrated as [8]:

$$S^{u}(t) = \sqrt{E_u} \sum_{-\infty}^{\infty} d_j^{u} \sum_{n=0}^{N_c-1} C^{u}(n) P_t(t - jT_f - nT_c) \quad (2)$$

where $P_t(t)$ is the second-derivative, Gaussian UWB pulse that was transmitted shown in Fig. 1(a); d^u_j [-1, 1] is the modulated binary data transmitted by user (u); $C^u(n)$ is the PR code or spreading sequence assigned to the u^{th} user; N_c is the spreading gain and is equal to T_s/T_c, where T_s is the symbol duration and T_c is the chip duration; E_u is the pulse transmitted energy; and T_f is the frame interval more than 100 times longer than the pulse width (T_w) to reduce the inter-symbol interference (ISI) between the UWB wireless communication systems. The other spread spectrum technique is TH-UWB which uses BPSK modulation as described in [9]:

$$S^{u}(t) = \sqrt{E_u} \sum_{j=-\infty}^{\infty} d^{u}_{\left[\frac{j}{N}\right]} P_t(t - jT_f - C_j^{u} T_c - \tau^{u}{}_0), \quad (3)$$

where τ^u_o is the resource delay for the first user which caused asynchronous transmission 0 τ^u_o T_f and to avoid the waveform collision of users, and C^u_j [1, 2,…..N_c] is used to assign the users up to the number of chips (N_c). There is an additional time shift provided in the TH-sequence by $C^u_j T_c$ to the j^{th} pulse of the u^{th} user and $T_f = N_c T_c$, as illustrated in Fig. 1.(b).

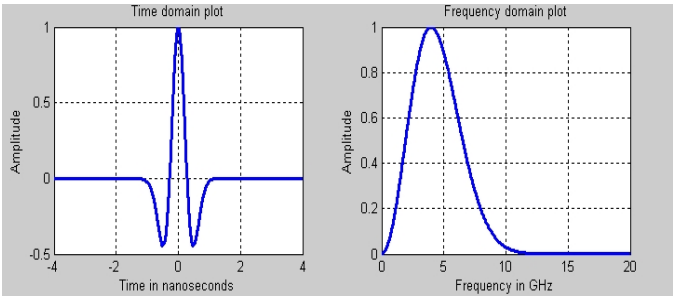

(a)

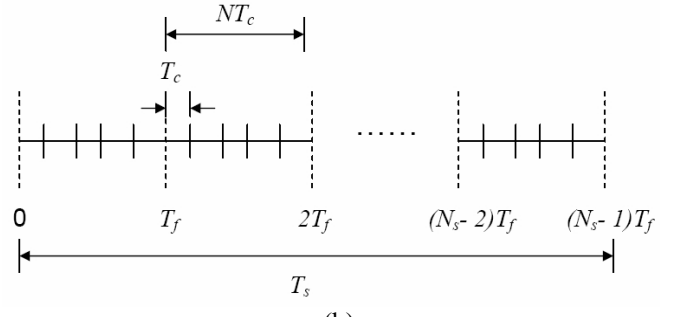

(b)

Fig. 1. (a) Time and frequency domains of a Gaussian UWB pulse; (b) THSS-UWB scheme for time divisions.

III. ANTENNA POWER RECEIVED

A 7.5GHz bandwidth is UWB system that spans the full band, thereby proving the capability of resolving more than 100 incident paths [9]. The center frequency (F_c) of the waveform can be determined from the minimum frequency (F_{min}) and maximum frequency (F_{max}) at the -10dB edges of the waveform spectrum, so F_c is given by:

$$F_c = \sqrt{F_{min} F_{max}} \quad (4)$$

when F_c is assumed to be 5 GHz. For indoor propagation, path loss (L_1) during one meter is $L_1 = 20\text{Log}_{10}(4\pi F_c/c)$, where c is speed of light in free space ($3\text{x}10^8$ m/s). Therefore, $L_1 = 26.4$ dB while the path loss is based on d meters separation distance between T_x and R_x is modeled as $L_2 = 20\text{Log}_{10}(d)$, when d = 4 m, L_2 = 12 dB and when d = 10 m, L_2 = 20 dB.

We considered that the antennas based on design described in this paper were used in transmitter (T_x) and receiver (R_x) of a UWB system with a gain of 4 dB from practical and simulated results. That is a mean receiver antenna gain (G_R = 4 dB) and transmitter antenna gain (G_T = 4 dB). The transmitted power for wireless, short-range, indoor systems was -41.3 dBm/MHz or 75 nW/MHz, so that the receiver power (P_R) can be calculated for 4m and 10m ranges by the following equation [9]:

$$P_R = P_T + G_T + G_R - L_1 - L_2 \ \text{(dB)} \quad (5)$$

IV. UWB INDOOR CHANNEL MODELS

IEEE's 802.15 4a report consider the standard channel models for indoor, multi-path propagation during line-of-sight (LOS) and non-line-of-sight (NLOS) [10]. The UWB system must capture with very fine resolution most of the multipath components that arrive in clusters and rays that caused by objects in the room. The four main wideband indoor channel models, i.e., CM1 0-4 m LOS, CM2 0-4 m NLOS, CM3 4-10 m NLOS, and CM4 which were generated to fit a 25ns root mean square (RMS) delay spread to represent an extreme NLOS multi-path channel, are introduced by the modified Saleh-Valenzuela (S-V) model (Table 2) with the values of the main parameters. The parameters are: cluster arrival rate ($\boldsymbol{\Lambda}$), ray arrival rate ($\boldsymbol{\lambda}$), cluster decay factor ($\boldsymbol{\Gamma}$) ,ray decay factor ($\boldsymbol{\gamma}$), standard deviation of cluster lognormal fading term ($\boldsymbol{\sigma}_1$), standard deviation of ray lognormal fading term ($\boldsymbol{\sigma}_2$), and standard deviation of lognormal shadowing term for total multi-path realization ($\boldsymbol{\sigma}_x$). The main channel characteristics that were used to determine the model parameters were: i) mean excess delay, ii) RMS delay spread, iii) number of multipath components that arrived within 10 dB of the peak multipath arrival. The standard channel impulse response (CIR) of the S-V model was modeled by:

$$h^{u}(t) = X_u \sum_{l=0}^{L-1} \sum_{k=0}^{K-1} \alpha^{u}{}_{k,l} e^{j\phi_{k,l}} \delta(t - T^{u}{}_{k} - \tau^{u}{}_{k,l}), \quad (6)$$

where X_u is a lognormal random variable, T_k is the arrival time for the k^{th} cluster and $\boldsymbol{\tau}_{k,l}$ is the arrival time for multi-path components (MPCs) or rays in the k^{th} cluster, $\boldsymbol{\delta}$ is a diarc delta function, $\boldsymbol{\alpha}_{k,l}$ is the fading gain coefficients of the l^{th} rays in the k^{th} clusters, and $\boldsymbol{\Phi}_{k,l}$ is uniformly distributed in (0 , 2π). For simplicity, CIR can be expressed as:

$$h^{u}(t) = X_u \sum_{l=0}^{L-1} \sum_{k=0}^{K-1} \alpha^{u}{}_{k,l} \delta(t - T^{u}{}_{k} - \tau^{u}{}_{k,l}) \quad (7)$$

Two independent, exponential PDFs were formulated to describe the distribution of the arrival times of the clusters and the arrival times of the rays, as shown in Figure 2, and their parameters are defined in Table 2.

$$p(T_l | T_{l-1}) = \Lambda \exp[-\Lambda(T_l - T_{l-1})], \quad l > 0 \quad (8)$$

$$p(\tau_{k,l} | \tau_{(k-1),l}) = \lambda \exp[-\lambda(\tau_{k,l} - \tau_{(k-1),l})], \quad k > 0 \quad (9)$$

$$|\alpha_{k,l}| = 10^{(\mu_{k,l} + n_1 + n_2)/20}, \quad (10)$$

where $n_1 \propto \text{Normal}(0, \sigma_1^2)$, and $n_2 \propto \text{Normal}(0, \sigma_2^2)$ are independent and correspond to the fading on each cluster and ray, respectively.

$$E\left[|\alpha_{k,l}|^2\right] = \Omega_0 e^{-T_l/\Gamma} e^{-\tau_{k,l}/\gamma} \quad (11)$$

$$\mu_{k,l} = \frac{10\ln(\Omega_0) - 10T_l/\Gamma - 10\tau_{k,l}/\gamma}{\ln(10)} - \frac{(\sigma_1^2 + \sigma_2^2)\ln(10)}{20} \quad (12)$$

where is a variable to produce power decay for the amplitude of each cluster and each multipath ray within the cluster, and $\boldsymbol{\Omega}_0$ is the mean energy of the first path in the first cluster. The shadowing term of the total multi-path energy, shown in Fig. 3, is captured by (X_u) and can be characterized as:

$$20\log 10(X_u) \propto \text{Normal}(0, \sigma_x^2) \quad (13)$$

The output of the UWB channel model is added with n(t), as its additive white Gaussian noise (AWGN) of power spectral density $N_0/2$ after the convolution is done between the transmitted signal and the response of the channel impulse. So, the received signal model r(t) can be formulated to obtain the general expression for received signal from user (u).

$$r(t) = X_u \sum_{l=0}^{L-1} \sum_{k=0}^{K-1} \sum_{u=0}^{U} \alpha^{u}{}_{k,l} S^{u}(t - T^{u}{}_{k} - \tau^{u}{}_{k,l}) + n(t), \quad (14)$$

where $S^u(t)$ is the transmitted signal by user (u), and, in order to avoid the loss of generality, the time delay for user (1) is assumed to be zero, i.e., $\boldsymbol{\tau}(0) = 0$. According to the FCC's 802.15.4a report and by using MATLAB software, Fig. 4 was constructed to show the characteristics of the impulse response for the four channel models with delay spreads of several nanoseconds (25 ns for CM1, 50 ns for CM2, 150 ns for CM3, and 200 ns for CM4).

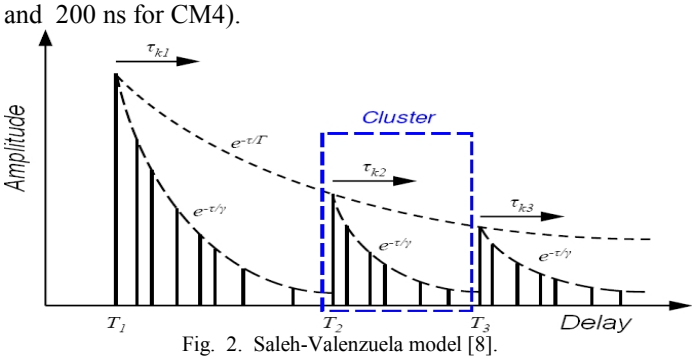

Fig. 2. Saleh-Valenzuela model [8].

Table 1. Key parameters that define the channel models.

Model Parameters	Λ (1/nsec)	λ (1/nsec)	Γ	γ	σ_1 (dB)	σ_2 (dB)	σ_x (dB)
CM 1	0.0233	2.5	7.1	4.3	3.3941	3.3941	3
CM2	0.4	0.5	5.5	6.7	3.3941	3.3941	3
CM3	0.0667	2.1	14	7.9	3.3941	3.3941	3
CM4	0.0677	2.1	24	12	3.3941	3.3941	3

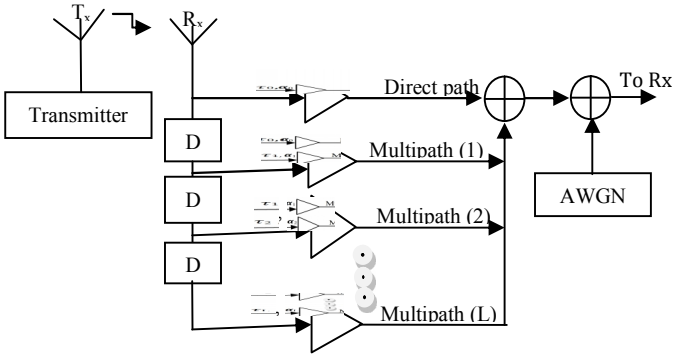

Fig. 3. Multipath channel for a wireless system.

978-1-4799-1532-3/13/$31.00 ©2013 IEEE

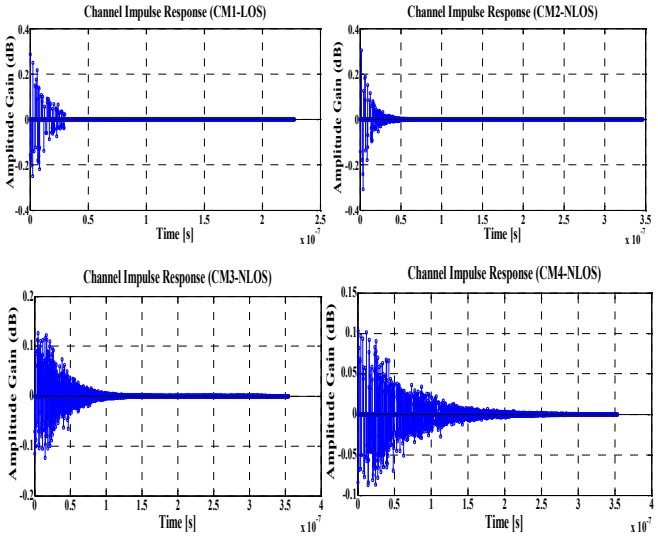

Fig. 4. Discrete time impulse responses based on channel models (CM1, CM2, CM3, and CM4).

V. CHANNEL CAPACITY FOR SINGLE AND MULTIPLE ANTENNAS

The gain of the antenna is one of the most important benefits of a wireless system that it increases the capacity of the channel without adding extra bandwidth or increasing the signal power at the transmitter. Increasing the capacity of the channel will support the improvement of the multiple-input, multiple-output (MIMO) technique in transmitters and receivers that determine the probabilities of error. In an MIMO system, we consider two random signal vectors, one for the input signal (s) to the channel and one for the output signal (q) from the channel [11]. Depending on Fig. 5 that shows the configurations of the selected antennas at the transmitter and receiver.

$$q = H\,s + w \tag{15}$$

where $s = [\,s_1, s_2, s_3, \ldots..s_M]^T$ is the transmitted signal vector up to M (number of omni-directional transmitted antennas), $q = [q_1, q_2, q_3, \ldots.q_N]^T$ is the received signal vector up to N (the number of omni-directional received antennas), w is the Gaussian noise vector with zero mean and equal variance, and H is the M x N channel matrix .

$$H = \begin{bmatrix} h_{1,1} \cdots h_{1,N} \\ \vdots \cdots \ddots \cdots \vdots \\ h_{M,1} \cdots h_{M,N} \end{bmatrix} \tag{16}$$

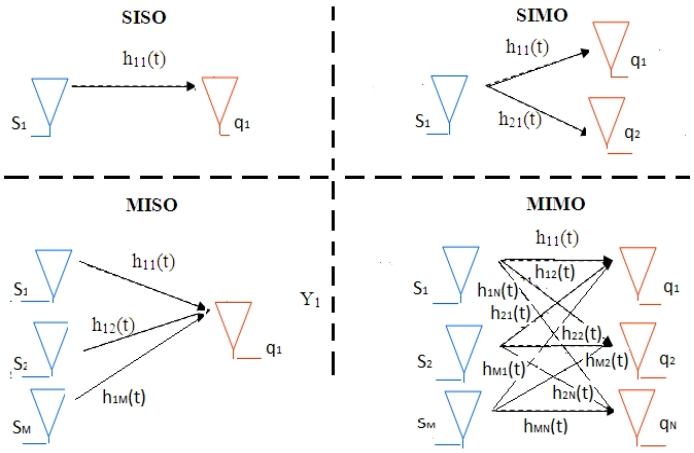

Fig. 5. Configuration of single and multiple antennas.

Assuming that the channels are noiseless means that their realizations are independent of each other. The capacities of the single-input single-output (SISO), single-input multiple-output (SIMO), multiple-input single-output (MISO), and multiple-output multiple-input (MIMO) systems (bits per sample) for indoor, UWB wireless bandwidth (B) are given by [12]:

$$C_{SISO} = B\log_2(1+\lambda \times SNR) \tag{17}$$

$$C_{SIMO} = B\log_2(1+SNR\sum_{n=1}^{N}\lambda_n) \tag{18}$$

$$C_{MISO} = B\log_2(1+\frac{SNR}{M}\sum_{m=1}^{M}\lambda_m) \tag{19}$$

$$C_{MIMO} = L \times B\log_2(1+\lambda \times SNR)\,, \tag{20}$$

where L is the number of channels, SNR is the signal-to-noise ratio, and **λ** is a non-zero eigenvalue of the M x N matrix. The signal-to-noise ratio (SNR) at the receiving antennas is defined as the ratio of the desired power of the received signal to 25% of the noise plus interference power, so that the SNR is related to and is proportional to antenna gain G(θ, **Φ**) when the noise distribution is uniform [12], where **Θ** is the elevation angle, and **Φ** is the azimuth angle for the antenna radiation patterns.

VI. RESULTS AND DISCUSSION

A. Simulated characteristics of the multi-path channel

978-1-4799-1532-3/13/$31.00 ©2013 IEEE

From the FCC's 802.15.4a report, the model parameters were designed to fit the results described in Table 1 with four scenarios for different distances between T_x and R_x. From Fig. 7, the characteristics of the impulse response for the four channel models with delay spreads of several nanoseconds led to considerable inter-symbol interference (ISI) if the pulses were spaced closely spaced in time for UWB. However, the existence of ISI and fading resulted in the receiver's having a high degree of diversity. The average power decay profiles of the four channel models, obtained from the MATLAB simulation, are shown in Fig. 6. These profiles show the amount of power that arrived within a confirmed delay interval and indicate that the variance in fading was independent of the delay time and that the fading depth increased as the delay increased for each channel model. In the LOS path, the fading delay was less than that in NLOS path, so that, with small delays, a few multi-path components arrive within one resolvable delay. The long delay spread excludes many different paths that the multi-path components could have taken, resulting in inter-arrival times between the multi-path components as a negative implication that tends to decrease the delay time. The average power received was distributed between a numbers of multi-path arrivals, which increased the complexity of the rake receiver for capturing most of the multi-path energy by collecting the arriving multipath components at different times. Fig. 7 shows the energy for 50 channels, which was distributed between a numbers of multi-path arrivals, so rake receivers must be designed to take advantage of that energy by capturing most of it. Capturing energy in this way for selected indoor environments is important in the investigation of office environments, airport hallways, and homes with different designs. The simulated results that define the relationship between the number of paths and the channel number are shown in Fig. 8 for the four channel models. These results describe the number of paths that must be collected to get 85% energy or more for each channel. This characteristic can be used beneficially in the design of indoor, multi-path receivers or to improve the reception of signals.

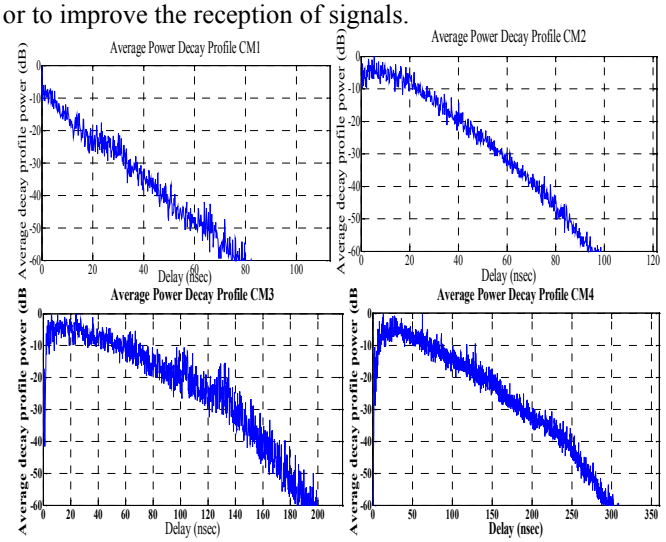

Fig. 6. Average power delay profile for channel models (CM1, CM2, CM 3, and CM4).

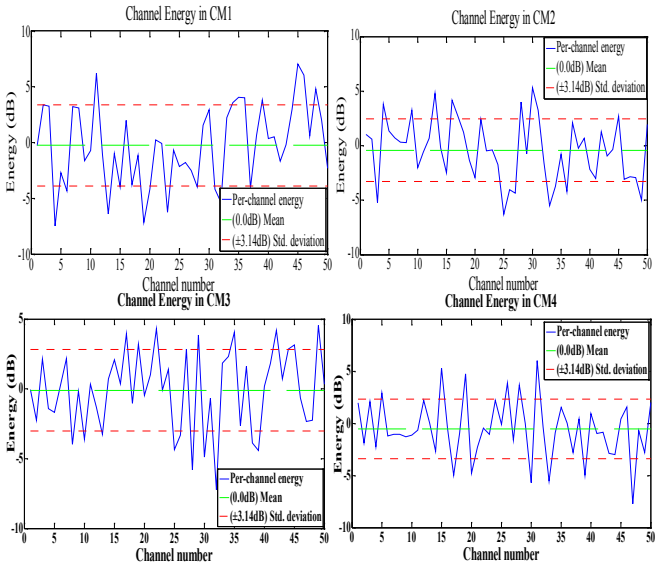

Fig. 7. Characteristics of channel energy determined using the channel models (CM1, CM2, CM 3, and CM4) for 50 channels.

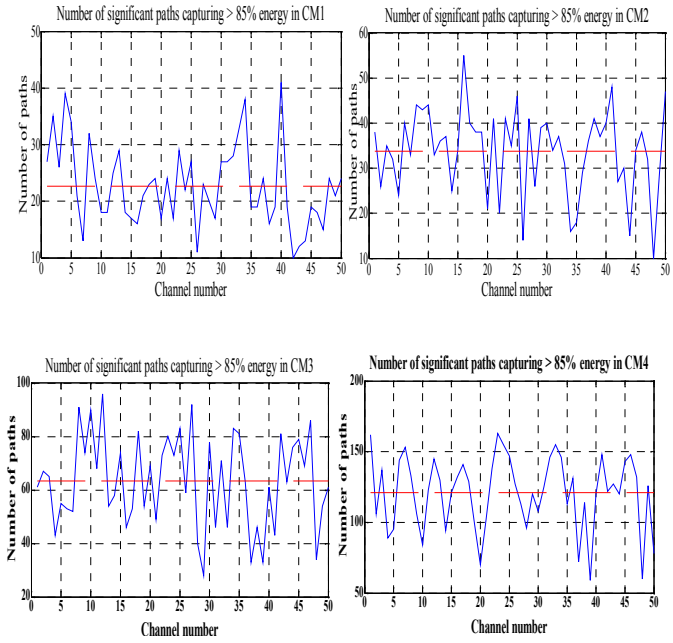

Fig. 8. Number of path characteristics that captured energy for channel models (CM1, CM2, CM3, and CM4).

B. *Simulated results of channel capacity*

Fig. 9 and Fig. 10 show 100 random channels to illustrate the results of the MATLAB simulations for flat-fading SISO, SIMO, MISO, and MIMO channels with SNR = 10 dB (depends on high gain of the antenna that was used). Table 2 illustrates the cumulative distribution function (CDF) of the capacities with different values of mean and 10% outage capacities for these channels. The performance of the MIMO system presented in Fig. 10 describes the increasing channel capacity attained by using the high-gain, multiple antennas at the transmitter and receiver for indoor wireless systems.

978-1-4799-1532-3/13/$31.00 ©2013 IEEE

TABLE 1. Simulated results of outage and mean bit rate capacities at M x N antennas

Channel System			10% outage capacity (pbs)	Mean Capacity (pbs)
SISO, SIMO, and MISO	M x N	1 x 1	0	1.9
		1 x 2	0.65	1.55
		2 x 1	0.65	1.55
		1 x 4	1.65	2.35
		4 x 1	1.6	2.4
		1 x 8	2.52	3.1
		8 x 1	2.5	3
MIMO	M x N	2 x 2	2.5	3
		4 x 4	6	8
		4 x 8	10	12
		8 x 4	10.5	12
		8 x 8	17.5	20
		8 x 16	26	27
		16 x 8	26.5	27
		16 x 16	46.5	48

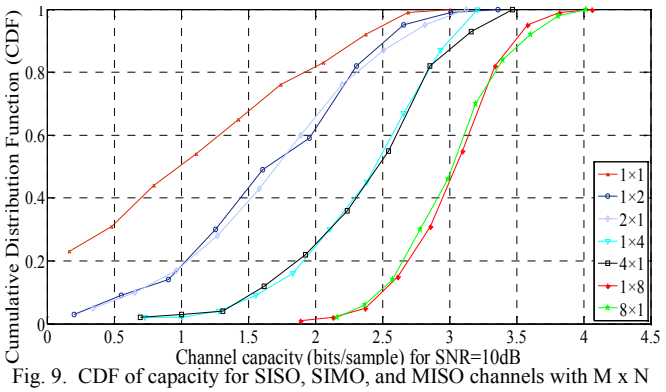

Fig. 9. CDF of capacity for SISO, SIMO, and MISO channels with M x N and SNR = 10 dB.

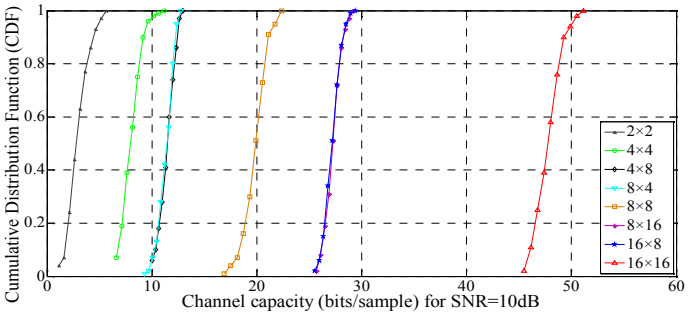

Fig. 10. CDF of capacity for MIMO channel with M x N and SNR = 10 dB.

VII. CONCLUSION

The high gain antenna can have a crucial role in the channel models that have 7.5 GHz bandwidth as defined by the FCC. In our research, we evaluated the capacity of the UWB channel for the SISO, SIMO, MISO, and MIMO cases. The beneficial effect on channel capacity of increasing the number of proposed, high-gain, receiving antennas was evidenced by the increased data rates of communication, making the system more suitable for indoor UWB-MIMO applications.

REFERENCES

[1] Ruonan Zhang and Lin Cai, ‘‘Modeling UWB Indoor Channel with Shadowing Processes,’’ Q shine Conference, Vancouver, Canada, August 2007.

[2] Shu-Han Liao, Hua-Pin Chen, Chien-Ching Chiu, and Chan-Lian, ‘‘Channel capacity of Indoor MIMO-UWB Transmission for Different Material Partitions,’’ Tamkang Journal of Science and Engineering, Vol. 14, No. 1, pp. 49-63, 2011.

[3] T. Kaiser, F. Zheng, and E. Dimitrov, ‘‘An Overview of Ultra-Wide-Band Systems With MIMO,’’ Proceedings of the IEEE, Vol. 97, No. 2, pp. 285-312, 2009.

[4] A. Sibille, C. Oestges, and Z. Alberto, ‘‘MIMO From Theory to Implementation,’’ Elsevier Inc., 2011.

[5] W. Q. Malik, and D. J. Edwards, ‘‘Measured MIMO Capacity and Diversity Gain With Spatial and Polar Arrays in Ultra Wideband Channels,’’ IEEE Trans. Commun., Vol. 55, No. 12, pp. 2361-2370, Dec. 2007.

[6] Y. Zhuo, L. Yan*, X. Zhao, and K. Huang, ‘‘A Compact Dual-Band Patch Antenna for WLAN Applications,’’ *Progress In Electromagnetics Research Letters, Vol. 26, 153-160, 2011.*

[7] H. Oraizi and B. Rezaei, ‘‘Combline Loadings of Printed Triangular Monopole Antennas for the Realization of Multi-Band and Wideband Characteristics,’’ Progress In Electromagnetic Research B, *Vol. 39, 179-195, 2012.*

[8] Huseyin Arslan, Zhi Ning Chen, and Maria Gabriella Di Benedetto,’’ Ultra Wideband Wireless communication,’’ John Wiley & Sons, Inc. , Hoboken, New Jersey, U.S., 2006.

[9] D. Gesbert, M. Shafi, D. Shan shin, P. J. Smith, and A. Naguib, ‘‘From Theory to Practice : an overview of MIMO space time coded wireless systems,’’ IEEE T.Select, Areas common, Vol. 21, no. 3, pp. 281-302, Apr. 2003.

[10] J. Foerster, et. al., ‘‘Channel Modeling Sub-committee Final Report on Channel Models for Ultra Wideband Personal Area Networks,’’ IEEE P802.15-02/490r1-SG3a, August 2012.

[11] Shuo Pan, ‘‘Capacity of MIMO systems for spatial channel model scenarios,’’ MSc. Thesis, The Australian National University, Canberra, Australia, June 2006.

[12] B. P. Lathi, and Zhi Ding, ‘‘Modern Digital and Analog Communication Systems,’’ International Fourth Edition, Oxford University Press, UK , 2010.

978-1-4799-1532-3/13/$31.00 ©2013 IEEE